

Identification and Inversion of Magnetic Hysteresis Using LabVIEW and MATLAB

Bernhard Gross, Martin Kozek, Hanns P. Jörgl¹

Vienna University of Technology

Keywords: magnetic hysteresis, model inversion, virtual instrumentation

Abstract

The sinusoidal magnetization of a sample material is difficult to achieve, since the magnetic hysteresis poses a strong nonlinearity. In order to find the proper input voltage, a feed-forward strategy with a hysteresis model identification and inversion is proposed. The classical Preisach model in the Everett formulation is used for this purpose and eddy current effects are also included. The control system consists of a laptop computer with a data acquisition card using LabVIEW and MATLAB. The user interface is programmed as virtual instruments. After an initial identification procedure the model, its inverse, and the proper input voltage for a desired sinusoidal magnetization are computed. The resulting application achieves accurate results, is easy to use, supplies the user with transparent and clear information, and adds the flexibility for automation or remote control.

1 Introduction

The experimental setup described in ASTM A 932/A 932M-95 [1] for measuring the magnetic characteristics of steel sheet samples is used for recording the magnetic hysteresis of the sample material. The magnetization of the material should be an undistorted sine-function with frequencies ranging from 10 to 500 Hz. In the original standard only analogue gauges are mentioned, however, virtual instrumentation provides a much more flexible and informative tool to control an experiment. Therefore, both the execution of the experiment as well as the de-magnetization of the sample and the processing of measured data should be achieved by virtual instrumentation.

The instruction for a sinusoidal magnetization is demanding since the magnetic hysteresis of a material requires a non-sinusoidal input voltage. Therefore, the sine-shape should be guaranteed using both feed-forward and feed-back control. The emphasis of this paper is placed on the realization of the feed-forward part of the control scheme. In order to demonstrate the feasibility of this concept, a model inversion of a combined electric and magnetic hysteresis model is utilized. Using a laptop-computer with LABView and MATLAB the parameters of the hysteresis model are automatically identified and the necessary magnetic field and the input voltage are computed accordingly.

The physical foundations of magnetic materials are relatively well understood, and a detailed description can be found elsewhere (e.g. [2]). The choice of a proper hysteresis model for a given purpose is critical for the present problem, and good overview over

¹ All authors are affiliated with the
Vienna University of Technology
Institute for Machine- and Process-Automation
Gußhausstraße 27-29 / 328
A-1040 Vienna, Austria
email:kozek@impa.tuwien.ac.at

different model types can be found in [9]. In the present application the classical Preisach model in the Everett formulation, as described in [4], was used. The main advantages are a comparatively simple implementation of the identification and inversion procedure, which is also the reason why this type of model has been frequently used for the compensation of hysteresis phenomena in actuators ([6, 7, 10, 11]). An extensive presentation of the Preisach model can be found in [3], and the identification methods are described in [5]. One of the main parts of the work was programming the Virtual Instruments (VI) used for the control and user interface. Aside from the manual from the manufacturer a good introduction to the programming language G may be found in [8].

The paper is structured as follows: In section 2 a short introduction to the principles and nomenclature of magnetic hysteresis is given and the mathematical model is derived. The identification and inversion principle is outlined. The following section 3 briefly describes the experimental setup and the hardware used in the experiments. In section 4 the software tools and their interaction as well as the user interface are presented. The model inversion is described in section 5 along with results from experiments explained in section 6. A short roundup of the main ideas concludes the paper.

2 Magnetic Hysteresis

2.1 Fundamentals

When a magnetic field – e.g. of a current carrying coil – acts on a material, both permanent and induced magnetic dipoles are oriented accordingly. This property is quantified by means of the magnetization M . The resulting magnetic induction is comprised of the part from the coil $\mu_0 H$ and of the part from the material $\mu_0 M$, which is also called polarization I :

$$B = \mu_0 (H + M). \quad (1)$$

The relation $B(H)$ is shown schematically in fig. 1. The magnetic induction increases according to the outer magnetic field H , caused by a growing number of oriented dipoles. Due to saturation a maximum magnetization M_S exists, which is the so-called saturation-magnetization. The total field can now only increase by the outer field from the coil (linear parts of the curve). A reduction of the magnetic field leaves a remainder of magnetization even when the outer field intensity is zero. This remanence B_r is the starting point for an inversion in the magnetic field. Only when the converse field has an intensity of H_c (coercive intensity) the overall magnetic induction is zero. For growing negative values of the outer field saturation occurs as before.

This nonlinear static relation between B and H including the past progression of the flux density is called the magnetic hysteresis. A very important dynamic effect is the expansion of the hysteric curve at higher frequencies due to eddy currents (see fig.2).

2.2 Model

The model inversion demands several properties of a hysteresis model:

- Simple and fast computation of flux density B and magnetization M , respectively.
- A wide range of materials where the model is valid (both magnetic hard and soft).
- Simple and robust identification of model parameters.

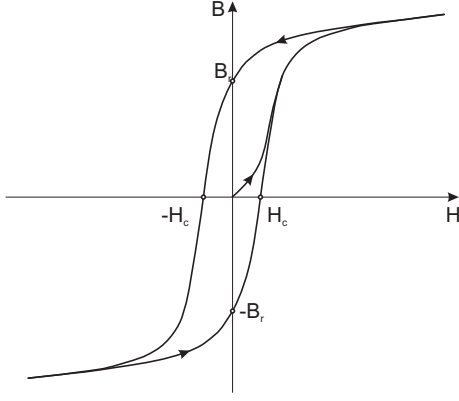


Figure 1: Major hysteresis loop

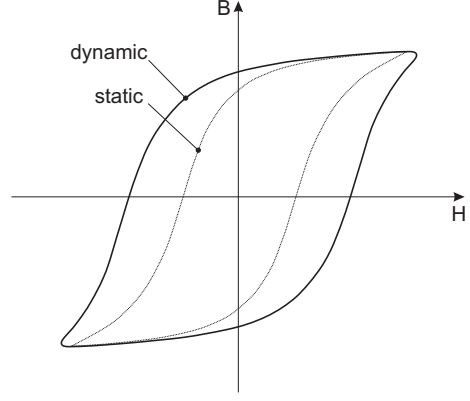


Figure 2: Dynamic loop

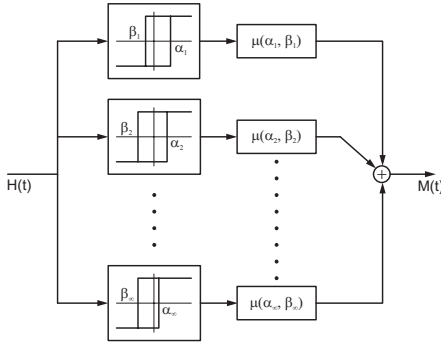


Figure 3: Preisach plane

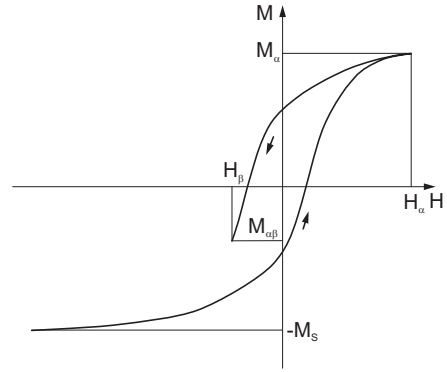


Figure 4: FOD curve

- The model must be invertible.

The Preisach model complies with all these demands in a harmonic way and is therefore chosen as proper model structure.

2.2.1 Classical Preisach Model (CPM)

The CPM defines the hysteresis loops by a parallel connection of individual hysterons (see fig.3). The hysterons are simple 2-state relays with hysteresis, where the upper switching point is α_i , the lower switching point is β_i , and the output is defined by

$$\phi(t) = \begin{cases} -1 & : H(t) \leq \beta \\ +1 & : H(t) \geq \alpha \\ \pm 1 & : \beta < H(t) < \alpha \end{cases} \quad (2)$$

Only hysterons with $\alpha \geq \beta$ are physically meaningful, due to their energy dissipating property. In the case $\alpha = \beta$ the hysterons may switch reversibel. The set of all possible hysterons P is defined by:

$$P = \{(\alpha, \beta) \in \mathbb{R}^2 \mid \alpha \geq \beta\}. \quad (3)$$

Without further details it is noted that the efficient computation is achieved by means of the Everett integral or Everett function

$$E(H_\alpha, H_\beta) = M_\alpha - M_{\alpha\beta}, \quad (4)$$

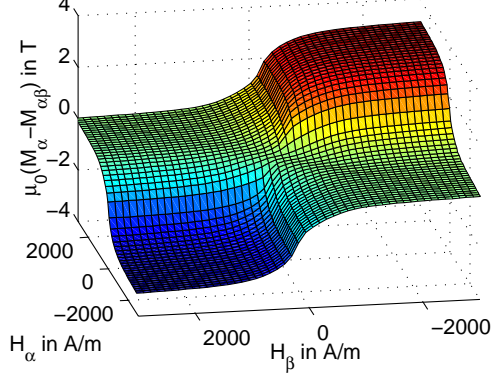


Figure 5: Everett map

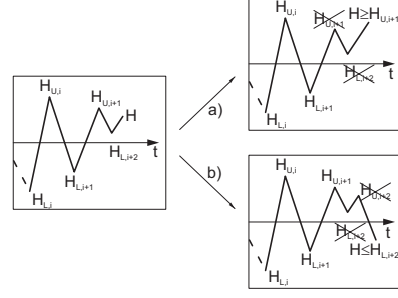


Figure 6: Wiping out property

which can be found by measuring the so-called First-Order-Descending (FOD) curves (see fig.4). The resulting hysteresis is then described by

$$M(H(t)) = -M_S + \sum_{i=1}^{k-1} E(H_{d,i+1}, H_{d,i}) + E(H(t), H_{d,k}) \quad (5)$$

The $H_{d,i}$ define the dominant extremes

$$H_d = \{H_{d,i}\} = \{H_{L,1} = -H_S, H_{U,1}, H_{L,2}, H_{U,2}, H_{L,3}, \dots, H_{U,m} \text{ oder } H_{L,n}\}, \quad (6)$$

which are subsets of all previous maxima

$$H_U(t) = \{H_{U,1}(t_{U,1}), H_{U,2}(t_{U,2}), H_{U,3}(t_{U,3}), \dots, H_{U,m}(t_{U,m})\}, \quad (7)$$

and minima

$$H_L(t) = \{H_{L,1}(t_{L,1}), H_{L,2}(t_{L,2}), \dots, H_{L,n}(t_{L,n})\} \quad (8)$$

These subsets are ordered both in time $t_{L,1} < t_{U,1} < t_{L,2} < t_{U,2} < \dots < t$ as well as in magnitude $H_{L,1} < H_{L,2} < \dots < H_{L,n} < H(t)$ and $H_{U,1} > H_{U,2} > \dots > H_{U,m} > H(t)$, respectively. If the current magnetic field is greater than a stored lokal maximum (fig.6,a), the stored maximum and all consecutive maxima and minima are wiped out. If the magnetic field is smaller than a stored minimum the situation is completely analogous (fig.6,b). This characteristic of the Preisach model is called the wiping out property and facilitates an efficient description of the magnetic state.

2.2.2 Identification

The identification of the CPM is accomplished by measuring multiple FOD curves which in turn defines the Everett map. For the measurements it is important to note that $H_\alpha \geq H_\beta$ holds and therefore only one half of the Everett map may be constructed by measurements. The remaining values may be completed using

$$E(H_\alpha, H_\beta) = -E(H_\beta, H_\alpha) \quad \forall H_\alpha < H_\beta. \quad (9)$$

2.2.3 Inversion

The Inversion of the CPM is carried out by computing the inverse of the Everett map F , defined by

$$F(M_\alpha, M_{\alpha\beta}) = H_\alpha - H_\beta. \quad (10)$$

the unknown magnetic field may be computed by

$$H(M(t)) = -H_S + \sum_{i=1}^{k-1} F(M_{d,i+1}, M_{d,i}) + F(M(t), M_{d,k}). \quad (11)$$

The computation is carried out similar to section 2.2.1, only H and M are interchanged.

3 Experimental Setup

The experimental setup depicted in fig.7 consists of the following components (see also fig.8)



Figure 7: Photograph of the experimental setup

- notebook & software
- multifunction I/O card
- control board PCB 1
- signal-conditioning board PCB 2
- power amplifier
- plant.

Data acquisition and control of the experimental setup was realized using the software LabVIEW 6.0 (NI-DAQ version 6.9.1). Although National Instruments provides software libraries for the direct hardware control with MATLAB, this configuration proved to be too slow ($1-3kS/s$) compared to the possible hardware sample rates. Therefore, the tasks of data acquisition and post-processing were split up between LabVIEW and MATLAB. LabVIEW clearly has advantages concerning speed of data acquisition and flexibility of measuring procedure, however, the effort and complexity of programming in LabVIEW's graphical programming language G seemed high to us compared to MATLAB.

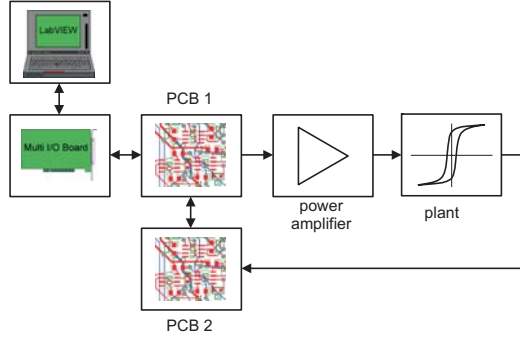


Figure 8: Block-diagram of the experimental setup

A DAQCard-6062E from National Instruments was used as data acquisition hardware and also for control input and output. It has 16 single-ended or 8 differential analogue inputs, respectively, with a resolution of 12 bit and a maximum sampling rate of (500 kS/s). The two analogue outputs feature update rates of up to (850 kS/s). Both inputs and outputs are designed for voltage levels up to $\pm 10\text{ V}$. Additionally, 8 digital TTL/CMOS compatible inputs/outputs are available, which were used for the control of the connected custom made control boards PCB1 and PCB2.

3.1 Control Board PCB1

PCB1 acts as an interface between measuring device and the experimental setup. On board are a Sliding Mode Controller for feed-back control (not treated here), two anti-aliasing filters which can be tuned using 8 bit for each filter, and several analogue switches for different control tasks.

The 8 digital inputs and outputs of the board are used as outputs only, and to provide a better guard for the hardware, they are separated from the data acquisition card by optoelectronic couplers. 4 outputs are used to tune the bandwidth and gain of the filters utilizing an additional control logic. Another 3 outputs are used for controlling the analogue switches, which govern the signal routing (filter on/off and switching between feed-back/feed-forward). The remaining output is dedicated to reset the integrator on board of PCB2.

3.2 Signal Conditioning PCB2

Board PCB2 is only built for signal conditioning purposes. It has 2 channels with the possibility of AC or DC coupling, respectively. Because the filter elements on PCB1 are only capable of maximal $\pm 5\text{ V}$ both channels are equipped with switchable 10:1 voltage dividers. This allows for the measurement of signals with voltage ranges as high as $\pm 50\text{ V}$. For protection of the filters an additional voltage limitation is implemented.

Channel 1 features the additional possibility of integrating the measured input.

3.3 Power Amplifier

The choice of an appropriate power amplifier must consider that measuring the FOD curves requires DC capabilities. The power amplifier utilized in the experimental setup is

manufactured by Brüel & Kjaer and is originally designed for driving electro-dynamical shakers. Nevertheless, it may be used for the current application with minor limitations.

3.4 Plant

The actual plant consists of a magnetic yoke (made of layered iron sheets), a mutual inductor (for the compensation of the magnetic air flux), a measuring resistor, and the power amplifier. The block-diagram is depicted in fig.9. The physical units of the measured

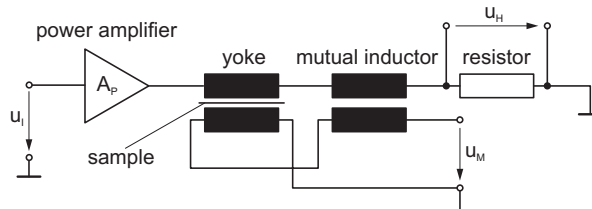


Figure 9: Plant

variables can be computed by

$$M(t) = \frac{1}{\mu_0 N_{Y_s} A_S} \int u_M(t) dt \quad (12)$$

and

$$H(t) = \frac{N_{Y_p}}{l_M R_H} u_H(t). \quad (13)$$

from the measured voltages u_M and u_H . N_{Y_p} and N_{Y_s} are the primary and secondary number of windings of the yoke, A_S is the cross-section of the sample, l_M is the length of the magnetic path inside the sample, R_H is the resistance of the measuring resistor, and μ_0 is the magnetic field constant.

4 Software

The software necessary for controlling the experiments essentially comprises two virtual instruments: *identES.VI* for measuring the FOD curves as a prerequisite for identification, and *PreiSin.VI* for the feed-forward control of the experiment. The interaction between MATLAB and LabVIEW and the course of an experiment is depicted in fig.10.

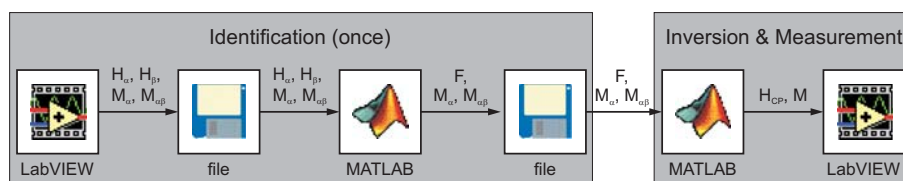


Figure 10: LabVIEW-MATLAB interaction

The identification of the hysteresis model is done as described in section 2.2.2 by measuring several FOD curves and consists of two steps. In the first step the Everett map is constructed using *identES.VI*, and in the second step the inverse of this surface is

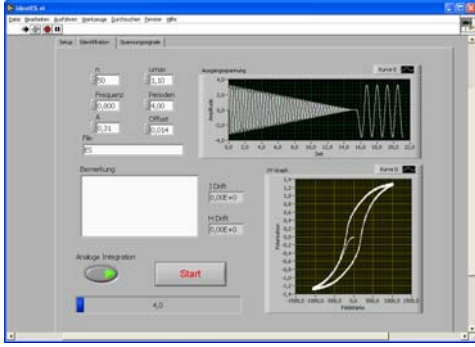


Figure 11: identES.VI

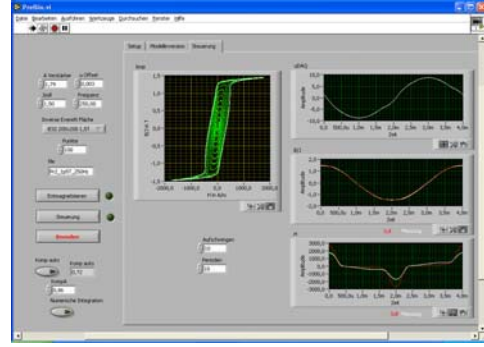


Figure 12: PreiSin.VI

computed. It should be noted, that the identification is only performed once for a given sample material, while the experiment may be conducted repeatedly using the same data from identification.

The user-interface of the above described identification-VI (fig.11) is structured into 3 tabs (alternative windows). In the setup-tab data for sampling, filters, plant parameter, and de-magnetization procedure can be supplied by the user. In the main-tab the frequency of the magnetization for identification, the number of points used for identification, the voltage levels, and the number of periods can be chosen. Additionally, the before measured FOD curve and a display for the progress of the experiment can be seen. In the third tab the measured raw voltage and the result of the averaging process can be found as a quick check-up.

After the identification has been started the appropriate number of FOD curves are measured. Once an individual FOD curve has been recorded, an average over all periods is computed and the necessary values H_α , H_β , M_α , and $M_{\alpha\beta}$ are extracted and stored in matrices. Then, the next FOD curve is being recorded. The resulting data structures in matrix form are stored on hard-disc in MATLAB-format using a MATLAB node inside the VI. This concludes the identification procedure.

The second step is the computation of the inverse Everett map $F(M_\alpha, M_{\alpha\beta})$, which is performed completely outside of LabVIEW using MATLABs computational power in vector/matrix calculations. The function *ES2iES.m* is tailored to perform this inversion and to save the data into another file in MATLAB-format.

The control of the experimental setup is finally done by the Virtual Instrument *PreiSin.VI* (fig.12). This VI consists also of 3 tabs, just like *identES.VI*. In this case the setup-tab is identical, but the desired amplitude and frequency of the sine-function can be chosen deliberately by the user. The resulting measurements and the inverted model are shown in different tabs.

Before the feed-forward experiment is started, the according inverse Everett map is loaded inside a MATLAB node, and the theoretically correct static magnetic field H_{CP} is computed considering the desired amplitude. This is accomplished by the MATLAB-function *CPM_E.m*. The magnetic field together with the magnetization M is handed over to LabVIEW. Finally, the necessary input voltage to the plant u_I is computed as specified in section 5, and this voltage is fed into the power amplifier.

The main advantages of a setup with a multi-functional data acquisition card as opposed to the setup described in the norm using individual gauges is the high flexibility, added information by efficient diagrams, and the possibility to automate or remote control the complete experiment.

5 Model Inversion

Based on the desired magnetization M and the appropriate magnetic field H_{CP} , which has been computed using the inverse hysteresis model, the magnetic induction results as

$$B = \mu_0 (H_{CP} + M). \quad (14)$$

In order to account for the approximate effect of eddy currents the actual necessary magnetic field becomes

$$H = H_{CP} + \frac{\sigma d^2}{12} \frac{dB}{dt}, \quad (15)$$

where d is the thickness of the sample and σ is the inverse resistance. The current in the primary circuit can be computed using the length of the magnetic path l_M , the number of windings of the primary coil of the yoke N_{Yp} , and the necessary magnetic field:

$$i = \frac{l_M}{N_{Yp}} H. \quad (16)$$

The necessary input voltage u_I can now be calculated, using the cross section of the sample A_S , the ohmic resistance of the primary yoke coil R_{Yp} , the measuring resistor R_H , and the mutual inductor R_{MI} , respectively, and the inductance L_{MI} :

$$u_I = \frac{1}{A_P} \left[N_{Yp} A_S \frac{dB}{dt} + (R_{Yp} + R_H + R_{MI}) i + L_{MI} \frac{di}{dt} \right] \quad (17)$$

6 Results

Using the software described in section 4 the performance of an experiment is straightforward and efficient. A laptop-computer with measurement-hardware is sufficient, no other measuring devices are needed. All signals and important physical quantities can be displayed or accessed easily. The course of an experiment can also be supervised, and measuring problems like artifacts can be identified on-line. Immediately after the experiment has been conducted all data is already formatted in correct physical units and ready for automated post-processing.

User interaction can be minimized, however, the flexible concept of the user interface allows direct access to all parameters for an expert user. Due to the virtual instrumentation, a remote control via TCP/IP of the complete experiment becomes possible.

In figure 13 the most important signals for 2 magnetic polarizations (1 and 1.5 Tesla) at 3 different frequencies (10, 100, and 200 Hertz) are plotted. The x-axis of each plot is scaled over one period regardless of the frequency.

In the first row, the magnetic polarization is depicted. The desired signal is a undistorted sine-function (continuous black line) and the measured polarization is in good agreement, especially for small to medium polarizations. With higher levels of polarization model deviations have a stronger impact and slight distortions cannot be avoided. The magnetic field depicted in the second row clearly shows a strong nonlinear behavior which is directly correlated to the hysteresis loop. The dependence on frequency is mainly caused by eddy currents, however, the implemented model for these dynamic effects does also contribute to the distortions visible in the magnetic polarization. The third row shows the measured input voltage which is close to a pure sine-function for high frequencies, regardless of the polarization. This effect can be explained by eq.17 where the part

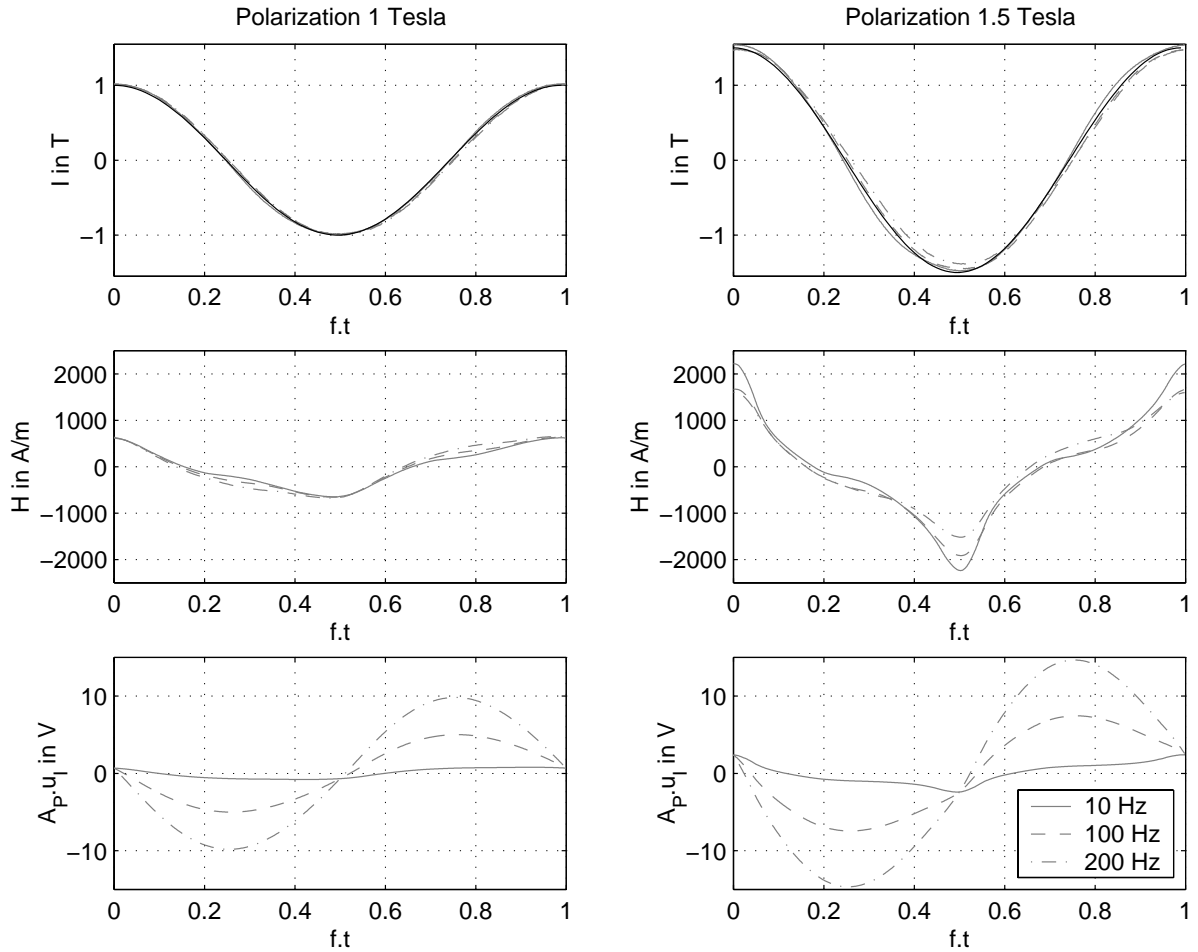


Figure 13: Experimental results. Left column: polarization of 1 Tesla, right column: polarization of 1.5 Tesla. Top row: magnetic polarization, second row: magnetic field, third row: input voltage. Results are plotted for 3 different frequencies: 10, 100, and 200 Hertz. The x-axis is scaled over one period regardless of the frequency.

$\frac{dB}{dt}$ becomes dominant for higher frequencies. For low frequencies the nonlinear behavior of the experimental setup is clearly visible in the input voltage.

Apparently, using only feed-forward control the main nonlinearities of the experimental setup were already removed for a wide variety of frequencies and polarizations and whatever distortions remain in the polarization could be compensated by means of an additional feed-back controller.

7 Conclusion

In this paper the problem of sinusoidal magnetization of a ferro-magnetic sample using virtual instrumentation VI is addressed. The main problem is the magnetic hysteresis of the material, which poses a strong non-linearity between the input voltage and the resulting magnetization. A combined feed-back and feed-forward approach seems to be very promising to overcome this problem for a wide range of input amplitudes and frequencies. Only the feed-forward part using a hysteresis identification and inversion method is treated in this paper.

A Classical Preisach Model in the Everett formulation is used for identification and the Everett map is the basis for the model inversion. The Everett map is measured using First Order Descending (FOD) curves, which are recorded during the initial identification phase of an experiment. After computation of the according input voltage the experiment can be started and the sinusoidal magnetization is achieved with a high level of accuracy even without feed-back control.

The overall control is done by a laptop-computer using LabVIEW and MATLAB and a DAQCard-6062E from National Instruments. Only two additional boards for signal conditioning and control are used as interfaces between laptop and experimental setup. The data input/output handling is accomplished by LabVIEW and more intensive computations are performed inside of MATLAB. This strategy has been proven necessary since on one hand the MATLAB libraries did not enable the use of high enough sampling rates, and on the other hand LabVIEW is not as well suited for intensive vector/matrix computations. The complete user interface is programmed as VIs.

The resulting application is easy and comfortable to use, provides a lot of information not only on the sample material but also on the course of the experiment, making it easier to find and resolve problems in the course of an experiment. The feed-forward control achieves very good results in guaranteeing a sinusoidal magnetization, and proves to be quite robust with respect to different materials, amplitudes, and frequencies.

Nonetheless, the programming of real-time applications using the G programming language of National Instruments requires considerable skill and knowledge, and some specific computational intensive parts of programming are still better done in alternate programs as MATLAB.

Future work should cover the development of a feed-back controller in order to guarantee stable performance under an even wider range of operating conditions, and possible refinements of the model considering dynamic effects.

References

- [1] ASTM. *A 932/A 932M-95 Standard Test Method for Alternating-Current Magnetic Properties of Amorphous Materials at Power Frequencies Using Wattmeter-Ammeter-Voltmeter Method with Sheet Specimen.*
- [2] Giorgio Bertotti. *Hysteresis in Magnetism.* Academic Press, 1998.
- [3] Edward Della Torre. *Magnetic Hysteresis.* IEEE Press, 1999.
- [4] T. Doong and I.D. Mayergoyz. On numerical implementation of hysteresis models. *IEEE Transactions on Magnetics*, 21(5):1853–1855, 1985.
- [5] Olaf Henze and Wolfgang M. Rucker. Identification procedures of Preisach model. *IEEE Transactions on Magnetics*, 38(2):833–836, 2002.
- [6] H. Hu and R. Ben Mrad. On the classical Preisach model for hysteresis in piezoceramic actuators. *Mechatronics*, 13:85–94, 2003.
- [7] Declan Hughes and John T. Wen. Preisach modeling of piezoceramic and shape alloy hysteresis. *Smart Materials and Structures*, 6:287–300, 1997.
- [8] Gary W. Johnson and Richard Jennings. *LabVIEW Graphical Programming.* McGraw-Hill, 2001.

- [9] F. Liorzou, B. Phelps, and D.L. Atherton. Macroscopic models of magnetization. *IEEE Transactions on Magnetics*, 36:418–428, 2000.
- [10] Samir Mittal and Chia-Hsiang Menq. Hysteresis compensation in electromagnetic actuator through preisach model inversion. *IEEE/ASME Transactions on Mechatronics*, 5(4):394–409, 2000.
- [11] Jürgen Schäfer and Hartmut Janocha. Compensation of hysteresis in solid-state actuators. *Sensors and Actuators*, 49:97–102, 1995.